PERGAMON

International Journal of Heat and Mass Transfer 42 (1999) 1979–1989

International Journal of HEAT and MASS TRANSFER

Experimental Nusselt numbers for a cubical-cavity benchmark problem in natural convection

W.H. Leong[1], K.G.T. Hollands*, A.P. Brunger[2]

Solar Thermal Research Laboratory, Department of Mechanical Engineering, University of Waterloo, Waterloo, Ontario, Canada N2L 3G1

Received 28 April 1998; in final form 25 August 1998

Abstract

Experimental natural convection Nusselt numbers are reported for a cubical, air-filled cavity that has one pair of opposing faces isothermal at different temperatures, T_h and T_c, the remaining faces having a linear variation from T_c to T_h. Average Nusselt numbers at the cold face are given for Rayleigh numbers Ra equal to 10^4, 10^5, 10^6, 10^7 and 10^8, and for three angles of inclination φ of the isothermal faces from horizontal: namely $\varphi = 0$, 45 and 90°. The 95% confidence limits on the measured Nusselt number Nu are typically 1% of the Nu. Unexpectedly, two Nusselt numbers were found at $\varphi = 0°$ and $Ra = 10^5$, depending on the initial conditions. The results are intended to provide data for a recently-defined benchmark problem in CFD.

Nomenclature

A_{hp} area of the electrically-heated plate, nominally equal to L^2
c_p specific heat of air at constant pressure
g acceleration due to gravity
k air thermal conductivity
L distance between the hot and cold faces of the cubical cavity (see Fig. 1)
LTP linear temperature profile
M number of a set of experiments to measure the same Nusselt number
Nu Nusselt number, $= 1+q_{conv}L/(k\Delta T\, A_{hp})$
n local slope of graph of log Nu versus log Ra
P air pressure
q heat-flow: with no subscript, q is the total heat flow (convection, conduction, and radiation) across the cubical cavity from the hot to the cold plate; q_b is the heat flow from the electrically-heated plate to the back plate, q_e is the electrical power delivered to the electrically-heated plate, q_s is the value of q when the air in the cavity is stationary: i.e. there is no convection
Ra Rayleigh number, $= g\beta\Delta TL^3\, c_p\rho^2/(\mu k)$
T absolute temperature: T_h and T_c are the temperatures of the hot and cold plates respectively (Fig. 1); T_m, $=(T_h+T_c)/2$, is the mean fluid temperature at which property values in Nu and Ra are to be evaluated.

Greek symbols
β coefficient of thermal expansion of air
ΔT T_h-T_c
μ air viscosity
ρ air density
φ angle of tilt of hot face of cavity from horizontal (see Fig. 1).

Superscripts
* relating to Ra*, a special nominal value of the Ra, like 10^4, 10^5, 10^6, etc.

1. Introduction

Benchmark problems have an important role to play in computational fluid dynamics (CFD). Once solved,

* Corresponding author. Tel: 001 519 888 4053; fax: 001 519 746 0852; e-mail: kholland@solar1.uwaterloo.ca

[1] Present address: Hatch Associates, 2800 Speakman Dr., Sheridan Science and Technology Park, Mississauga, ON, Canada L5K 2R1.

[2] Present address: National Solar Test Facility Canada, ORTECH Corp., 2395 Speakman Dr., Sheridan Science and Technology Park, Mississauga, ON, Canada L5K 1B3.

0017–9310/99/$ - see front matter
PII: S0017–9310(98)00299–3

they form a reference point for code development and validation. A benchmark problem should be capable of simple statement—yet it should challenge the best current codes, which means that new benchmark problems need to be defined periodically. Preferably the new problems should be physically-realizable, so that comparisons can be made with laboratory measurements.

Some popular benchmark problems have not been physically-realizable. A case in point is the problem of the 2D flow of air in a square cavity with isothermal vertical walls and adiabatic horizontal walls (side-walls) [1]. Le Quere [2], who has provided extensive solutions, noted that "for several reasons, this problem could ultimately prove to be without physical meaning." The lack of physical meaning stems from the impossibility of the adiabatic boundary condition [3] and (since the 2D flow could be unstable to 3D disturbances) from the 2D flow specification [4].

Despite the success of this rather unphysical problem, there are good reasons why future benchmark problems should be physically-realizable. For example, some physical aspect, such as the possibility of 3D flow, may be missing in the fundamental equations, or the flow may be bistable and the code is converging onto only one of the two solutions. Such benchmark measurements would be most useful for modelling transition and fully-turbulent flows: short of direct numerical simulation, it will be necessary to model the turbulence, and since modelling laws for buoyancy-driven turbulence are embryonic, the need to test against experimental measurements becomes paramount.

Close agreement between computed and measured convection in cavities has not generally been found in the past [5–11], in the main because simulated and experimental side-wall boundary conditions did not exactly match. The exception is the work of Hamady et al. [9], who achieved $\pm 3\%$ agreement for the Nusselt number. But they used their experimentally-measured sidewall temperature distribution as the boundary condition in the CFD code, rather than an idealized boundary that one would expect to find in a benchmark problem statement. While their findings constitute very useful knowledge, the method is not consistent with the basic idea of a benchmark, in which the model should be simply-stated and independence of any experimental measurements[3].

Because of the need for a physically-realizable benchmark problem and the long history of the square-cavity problem, it seems wise to build a new, physically-realizable problem on that foundation. In a companion paper to this one, Leong et al. [12] examined some suitable problems and found the most suitable to be natural convection in a cube with two opposing faces isothermal and the remaining four walls (called the side-walls) having a linear temperature variation from the cold face to the hot face, as shown in Fig. 1. They defined, in fact, three benchmark problems: one with hot (or cold) face

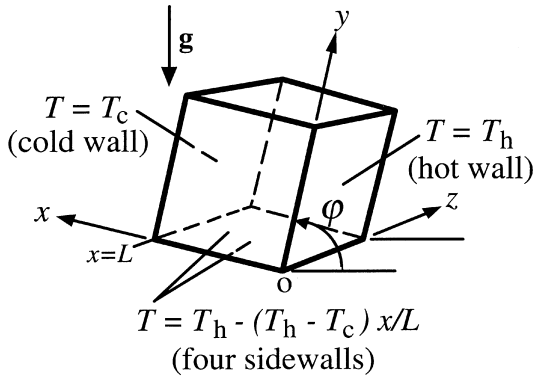

Fig. 1. Sketch defining the cubical cavity benchmark problem.

vertical (as in the square-cavity problem), one with it horizontal, and one with it inclined at 45°. They recommended air as the fluid, because its properties are closely-known, because its pressure can be easily varied (allowing a wide Rayleigh number range to be covered with a single physical model), and, finally, because its low thermal conductivity means that one can achieve the linear profile by making the side-wall of a good conductor.

Leong et al. [12] described an apparatus built up to realize the specified problem, and demonstrated the practical achievement of the linear profile. Taking the average Nusselt number, *Nu*, as the principal measured parameter, they suggested that the accuracy in *Nu* needed to be about 1% or better for the results to be useful for testing codes. They described an experiment aimed at achieving this accuracy, and demonstrated its fulfilment at a Rayleigh number *Ra* of 40 000. Because of length limitations, their results at higher Rayleigh numbers were not given.

[3] The comparisons achieved by Hamady et al. [9] on a 'complex' benchmark are appropriate when the same research group is doing both the CFD modelling and the experiments. But by keeping to 'simply-stated' benchmarks, the research community will promote the specialization of efforts that is needed to advance the science. That is, if some workers specialize in producing experimental results and others in developing computational models, specialized skills can be developed with greater focus, and moreover the comparisons can be more objective. 'Complex' benchmarks that 'fall-out' of a particular experiment (in the sense that the wall-temperature boundary condition of Hamady et al. [9] fell out of the peculiarities of their experiment) are not only difficult to characterize for the CFD modellers; they also make interlab comparisons very difficult, because the temperature boundary conditions that fall out of one lab's experiment are unlikely to match those that fall out of another lab's apparatus.

The results at higher Rayleigh number are now given in the present paper. Thus, average (cold-face) Nusselt number results, accurate to within about 1% error (95% confidence) are reported here for $Ra = 10^4$, 10^5, 10^6, 10^7 and 10^8, for each of the three values of angle φ. The results are compared to related computed values from the literature [2, 10, 13], and although the current literature contains no studies that exactly matched our boundary conditions, these comparisons throw light on the effects of 2D vs 3D flow and of the adiabatic vs the linear temperature boundary condition. Measured Nusselt numbers at $\varphi = 45^\circ$ were generally higher than those at both $\varphi = 0^\circ$ and $\varphi = 90^\circ$, a rather unexpected finding. Another unexpected finding was that when φ was set equal to 0° and Ra to 10^5, we observed two distinct Nusselt numbers, depending, apparently on the initial condition of the experimental set-up. The two Nusselt numbers differed by about 10%, and so resolving them was within the capabilities of the experiments. CFD simulations aimed at exploring this finding revealed that there are indeed two solutions at the condition $\varphi = 0^\circ$, $Ra = 10^5$. (No further CFD simulations were performed as part of the present study, whose main function is to provide experimental data for other studies.)

To obtain results specially-suited to CFD comparisons, we departed from the usual experimental procedure of taking measurements at many values of Ra and then fitting a curve through the data. Rather, we concentrated on making repeated measurements at (or very close to) a few specified Rayleigh numbers (denoted by Ra^*), such as 10^5, 10^6, 10^7, etc., and then averaging the results. This made the results suitable for direct comparison with the results of CFD codes, which are generally reported in the same way. The standard deviation of the repeated measurements was used in determining the random error in the Nusselt numbers.

2. Experiment

Most of the details of the apparatus and method are given by Leong et al. [12]. We provide here only a brief summary, adding details peculiar to the additional experiments reported here.

2.1. General layout

Shown in Fig. 2, the experimental cube model had side-length L nominally equal to 127 mm. It contained a heat flux meter, an electrically-heated plate, and two identical 'hemi-cubes', the latter two joining along a parting-line to form the cube after assembly. The 'hot-plate' was heated to about 307 K and the 'back-plate' cooled to about 300 K, each by water streams passing through tubes soldered to their rear faces. The model was contained in a pressure vessel, the pressure of which is controllable from about 100 to about 1 MPa, thus making the Rayleigh number controllable from about 100 to about 2×10^8.

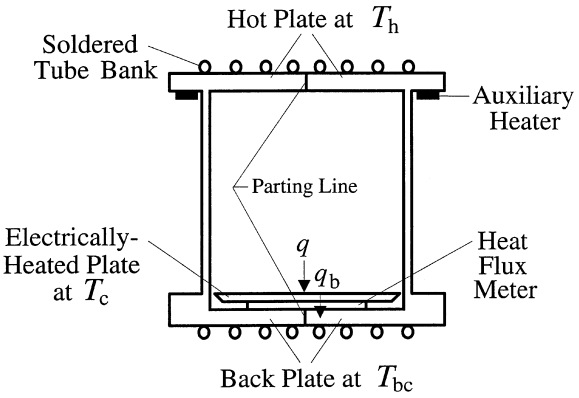

Fig. 2. Sketch of experimental apparatus in central cross-section.

2.2. Linear temperature profile

Four strategies led to achieve the linear profile on the side-walls. The first was placing the parting-line parallel to, rather than transverse to, the heat flow (this avoided temperature jumps due to contact resistance). The second was making the side-wall thick enough (it was 3.18 mm thick) to ensure a linear temperature distribution. Unfortunately, because of the constriction resistance where the side-wall meets the hot-plate and that where the side-wall meets the back-plate, this linearity did not extend from T_c to T_h. This led to the third strategy, which was applying a small amount of electrical heating (via an imbedded electrical wire) where the side-wall meets the hot plate (Fig. 2), and the fourth strategy, which was adjusting the heating to the electrically-heated plate so as to make its temperature equal to the temperature of the side-wall at the corner where they meet. With these strategies in place, the side-wall temperature deviated from the sought linear profile by less than 0.05 K. The last two strategies meant that the electrically-heated plate was actually at the cold end of the cavity, rather than the hot end, where one would find it in the standard guarded heat-plate method.

2.3. Heat flow measurement

The heat q carried to the cold face from the air is (except for radiation) the sought heat flow needed in the Nusselt number. From an energy balance, it is equal to the heat flow q_b passing through the back of the electrically-heated plate minus the rate q_e of electrical energy supplied to the electrically-heated plate: $q = q_b - q_e$. The heat q_e is easily measured, and the heat q_b can be determined from the heat calculated from the e.m.f of the heat

flux meter, which has been calibrated in situ. This, in basic terms, is the technique used to measure the heat flow q. In fact, the quantity actually entered into the Nusselt number is the excess of q over the corresponding value of q (denoted q_s) applying when the air is stationary and no convection is present. Thus we determined the Nusselt number Nu from

$$Nu = 1 + (q - q_s)L/(k/A_{hp}\Delta T) \quad (1)$$

with q_s being determined when the air is stationary, a condition established by having the pressure low and heating from above, i.e. by putting $\varphi = 180^\circ$. This procedure also eliminates the radiative transfer from further consideration.

The method for determining q from $q = q_b - q_e$ has the difficulty that if q becomes greater than q_b, q_e must be negative, and, coming from an electrical source, it is impossible to make it negative, so the method fails. In our experiments we increased the Rayleigh number in steps, each step resulting in an increase in Nu and hence in q. During this process, q_b remained more or less constant, and thus a point was eventually reached where q exceeded q_b. For our (original) apparatus, this point was reached when Ra was between 10^6 and 10^7. To accomplish the measurements at $Ra = 10^7$ and 10^8, we changed the heat-flux meter, replacing it with one of about one-third the thermal resistance of the original one. (This one was one third the thickness of the original one, and so a circular aluminium disc was added to the space between the back-plate and the electrically-heated plate to make up the spacing.) As a check on the integrity of the heat-flux measurement technique, the Nusselt number measurements at $Ra = 10^6$ were performed with both heat-flux meter arrangements, and the Nusselt numbers compared. They agreed to within about 0.6%, which was within the experimental uncertainty of the Nusselt number measurement.

2.4. *Setting of* Ra

In an experiment, it is impossible to set the Rayleigh number precisely equal to a particular Ra^*, like 10^m (where $m = 4$, 5, 6, 7 or 8); it is therefore necessary to determine the Nusselt number at this value from a set of measurements made with Ra in the close vicinity of Ra^*. Each measurement is corrected by the factor $(Ra^*/Ra)^n$ to bring it to the desired Ra^*. Here n is the local slope of the log Nu vs log Ra curve, which is determined from measurements at the next lowest and next highest Ra^*: for example if the Ra^* of interest is 10^6, n would be determined from the Nusselt numbers, Nu_5 and Nu_7, at 10^5 and 10^7 respectively, as follows: $n = \frac{1}{2}\log_{10}(Nu_7/Nu_5)$.

The error in this Nu is made up of two parts. The first is the bias error, which is established by the errors in the instruments and similar considerations; it includes the errors associated with the properties of air and the uncertainty in n. The factors entering into the bias error are given by Leong et al. [12]. The second component of the error in Nu is the random error, which is determined from the standard deviation of the M independent measurements of the (corrected) Nu in the immediate vicinity of Ra^*, and from the appropriate Student's t-multiplier.

Choosing to make $M = 18$, we carried out 18 Nusselt number measurements at each combination of Ra^* and φ. These were at various settings for the temperature difference ΔT, and mean temperature T_m, the pressures always being adjusted to make the Rayleigh number very close to (within 1% of) the desired Ra^*. To get the 18 measurements, three repetitions were made at each of the six permutations of $\Delta T = 4.5$, 6.2 and 9.7 K and $T_m = 298$ and 308 K, each repetition having a slightly different pressure. As was explained earlier, at $Ra = 10^6$, two different sets of measurements were made, each with a different heat flux meter. These two sets were merged and treated as a common set, so M was equal to 36 at $Ra = 10^6$. From now on, the superscript on Ra^* will be deleted as understood.

3. Results

The Nusselt number results are listed in Table 1 at each combination of Ra and φ, along with their corresponding 95% confidence limits of uncertainty.

3.1. *Results for* $\varphi = 90^\circ$

In Table 2, the results at the vertical position, $\varphi = 90^\circ$, are compared with available CFD solutions of allied problems. The third column gives the results that Raithby and Wong [13] obtained for the square cavity in 2D flow with the side-wall temperature running linearly from T_c to T_h, which we shall denote here as the linear temperature profile, or LTP, boundary condition. The fourth column gives recent solutions of Le Quere [2] for the well-known

Table 1
Measured Nusselt number results at the three angular settings

	Nu		
Ra	$\varphi = 0^\circ$C	$\varphi = 45^\circ$C	$\varphi = 90^\circ$C
10^4	1.246 ± 0.013	1.614 ± 0.015	1.520 ± 0.015
4×10^4	2.018 ± 0.017	2.650 ± 0.027	2.337 ± 0.020
10^5	3.509 ± 0.035	3.492 ± 0.034	3.097 ± 0.028
10^5	3.916 ± 0.042	—	—
10^6	7.883 ± 0.091	8.837 ± 0.101	6.383 ± 0.070
10^7	15.38 ± 0.19	17.50 ± 0.21	12.98 ± 0.16
10^8	31.22 ± 0.43	34.52 ± 0.42	26.79 ± 0.34

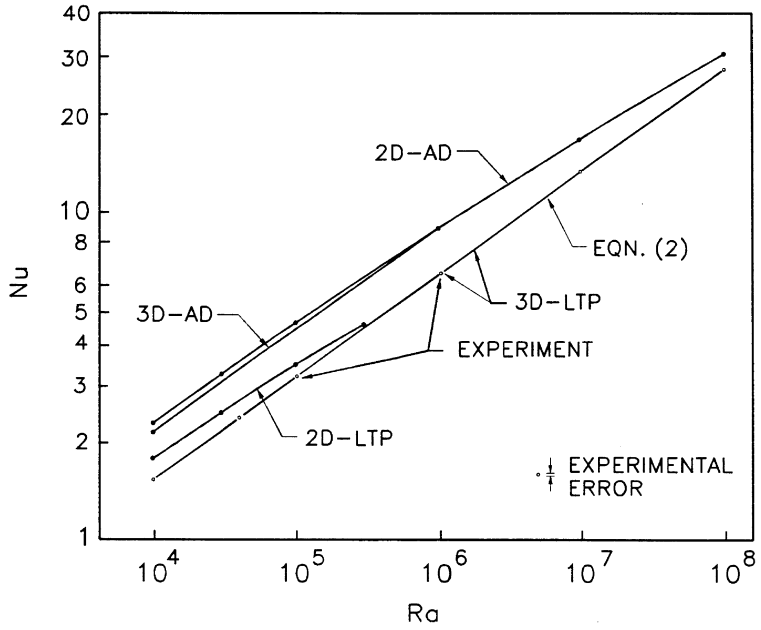

Fig. 3. Plot of the experimental results at $\varphi = 90^\circ$, and some computed results for allied problems from the literature. The curve marked EXPERIMENT (3D-PC) is the present experimental result; 2D-AD is Le Quere's result [2] for 2D flow in a square cavity with adiabatic side-walls; 3D-AD is Fusegi et al.'s result [10] for 3D flow in a cubical cavity with adiabatic side-walls; and 2D-LTP is Raithby and Wong's result [13] for 2D flow in a square cavity with linear temperature profile side-walls.

benchmark problem [1] of the square cavity in 2D flow with adiabatic side-walls. The fifth lists the fully 3D solutions of Fusegi et al. [10] for flow in a cubical cavity with adiabatic side-walls. While all three of these CFD solutions are for situations different from that of the problem reported on here, they are close enough to warrant comparison. Figure 3 is a plot of the data in Table 2.

In all cases, the CFD solutions give greater heat transfer than the observed heat transfer. The CFD-computed curve that runs closest to the experimental curve is that for the 2D flow, LTP case. Since the present experiments also have the LTP boundary condition, it seems that the thermal boundary condition is more decisive in fixing the heat transfer than the whether the flow is 2D or 3D. That the Nusselt numbers should be higher in 2D flow is perhaps to be expected, because the experimental cavity has additional side-walls along which the fluid experiences additional drag, thereby restraining total convective motion. This observation is consistent with the

Table 2
Comparison of Nusselt number results at $\varphi = 90^\circ$ with CFD results on related problems from the literature

		Computed *Nu* for		
Ra Cubical cell	Measured *Nu* LTP side-walls	2D flow, square cell, LTP side-walls [13]	2D flow, square cell, adiabatic side-walls [2]	3D flow, cubical cell, adiabatic side-walls [10]
10^4	1.521	1.75	2.24	2.10
3×10^4	—	2.41	3.14	—
4×10^4	2.337	—	—	—
10^5	3.103	3.40	4.51	4.361
3×10^5	—	4.47	—	—
10^6	6.389	—	8.83	8.77
10^7	13.00	—	16.52	—
10^8	26.83	—	30.22	—

fact that, of the top two curves, the 3D Nusselt number lies below the 2D Nusselt number, an observation also made by Fusegi et al. [10]. It appears, however, that the CFD simulations may in fact cross the line of the experimental data, rather than being asymptotic to it. This as well may be explainable. At very high Ra the eddies are much smaller than the length-scale of the cavities, so additional side-walls have a much less constraining effect. At the same time, the 'real world' of the experiments will allow for eddy motion in the third dimension, and hence the flow will be less constrained than that in the 2D simulations; this can lead to greater convective motion and higher heat transfer. Similar arguments could be made with respect to the top two curves, although it is more difficult to say whether the curves are asymptotic or crossing.

The CFD simulations assuming adiabatic side-walls are consistently higher than the LTP side-wall results, regardless of whether the latter are experimental or computed. That adiabatic side-walls produces more heat transfer across the cell than LTP side-walls is well-known and has to do with the more constraining effect of a side-wall of specified temperature as compared to an adiabatic side-wall. On the other hand, that the relative difference between the experimental and the 2D CFD simulations decreases with increasing Ra is an interesting observation that can probably be explained by the above-mentioned additional freedom allowed in the real-world 3D situation and also by the possibility that the simulated solutions calculated the steady solutions, whereas in the real-world, oscillatory flow may easily be taking place. Because of the latter effects, it is quite possible that these two curves will cross at higher Ra as well. (It should be noted, however, that previous studies have indicated that the flow should not become turbulent until Ra is approximately 10^8 [15].)

To complete these comparisons, it is instructive to discuss here the experimental data of Hamady et al. [9], who measured the Nusselt number for a square cell with experimental boundary conditions consisting of an insulated plexiglas sheet that provided neither the LTP nor the adiabatic boundary condition. Their results were found to lie between the values in the third and fourth columns in Table 2; i.e. they were bounded by the square-cell CFD simulations for adiabatic and LTP side-walls. For example, at $Ra = 10^5$, the Nusselt number from Hamady et al. [19] (as given by their correlation equation) is 4.14, which is roughly half way between the values of 3.40 and 4.51 given in Table 2. In comparing this Nusselt number of 4.14 with the present experimental one of 3.103, we note that there are three reasons for the difference: the different cavity shape (cubic vs square), the different side-wall materials (copper vs plexiglas) and different ways of heat sinking the side-walls into the hot and cold plates. It would seem that the differences in the side-walls is the over-riding reason for the difference in Nusselt numbers. These comparisons underline the importance of specifying an achievable side-wall boundary condition in the benchmark problem definition.

As is clear from Fig. 3, the present experimental data fall almost precisely along a straight line when plotted on a log-log plot; they are fitted by the single equation:

$$Nu = 0.08461 Ra^{0.3125} \quad 10^4 \leqslant Ra \leqslant 10^8 \tag{2}$$

to within the very low tolerance of 1% maximum deviation, which is of the same order as the experimental uncertainty.

3.2. Results for $\varphi = 0^\circ$

The results for $\varphi = 0^\circ$ are plotted in Fig. 4a. The results at $Ra = 10^5$ were found to fall into two sets, one with Nu approximately equal to 3.5 and one with Nu equal to 3.9. Because the difference between these two sets was greater than the resolving power of the experiments, the difference could not be put down to random error. The two sets were therefore kept separate, and an average was taken over each set. These are the two values reported in Table 1 and plotted in Fig. 4a for $Ra = 10^5$. There were eight data point at $Nu \approx 3.5$ and ten at $Nu \approx 3.9$, and the errors shown are in each case based on the corresponding number of observations; thus $M = 8$ or 10, depending on the case.

On examining the data to see if any particular experimental circumstance would decide which case (or mode) would in fact be observed, we found that the ΔT setting had no deciding effect, but the mean temperature T_m setting had an important effect: generally the $Nu \approx 3.5$ mode tended to be observed with $T_m = 298$ K and the $Nu \approx 3.9$ mode tended to be observed with $T_m = 308$ K. On the other hand, T_m was not fully decisive in determining which mode would be observed. Once a particular mode had developed, the heat transfer would not change to that of the other mode: it remained stable at the mode.

Because this result was rather unexpected and in view of the fact that the Rayleigh number was just low enough for the flow to be modelled with current commercial codes, we decided to simulate the flow at $Ra = 10^5$ with a CFD code, to see what light this would throw on the phenomenon. Prior work [16–19] on CFD simulations of cubical and quasi-cubical cavities heated from below have indicated that there are a number of possible different flow patterns, depending on the aspect ratio of the cavity, the Prandtl number, the sidewall boundary condition and the Rayleigh number. Moreover, even for a given specification of these various parameters, the flow structure may still not be unique: two or more different stable flow patterns may satisfy the steady-state equations of motion. Some of the patterns that have been described [16–19] are (i) single or double cells with the cell axis parallel to one of the side-walls, (ii) single cells with the axis along a diagonal, (iii) a toroidal ring vortex (also

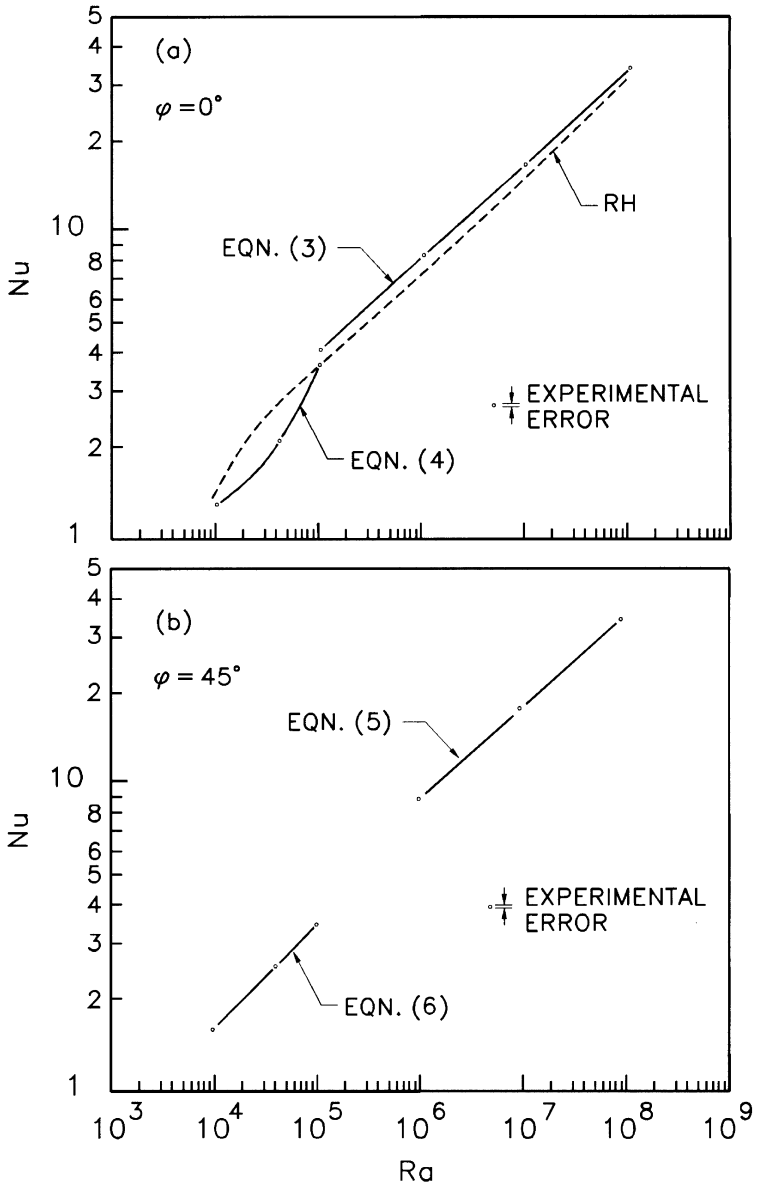

Fig. 4. Plot of results for $\varphi = 0$ and 45°. Dashed curve marked RH is a plot of a multi-Prandtl number multi-geometry correlation equation [20, 21] for enclosures heated from below.

called bimodal flow) where flow rises in the central region and falls along the walls, or vice-versa and (iv) a transition flow between the last two. These different flow structures may yield different Nusselt numbers [16].

The details of the CFD code we used in the present study were the same as those used by Leong et al., and are described in the appendix to that paper—the air properties being treated as constant in these particular simulations. The initial conditions were that the velocity field was zero and the temperature was uniform throughout the cavity, at the mean temperature. Only one side of the cavity was simulated, it being assumed that the flow would be symmetric about a central plane parallel to one of the side-walls. (This was a significant assumption, but as will be seen, it did not preclude the needed result.) Three simulations were performed, with grid sizes of $15 \times 15 \times 7$, $30 \times 30 \times 14$ and $60 \times 60 \times 28$ respectively. In the $60 \times 60 \times 28$ grid size simulations, the solution converged only very slowly, and in an oscillatory manner, and to achieve solution in a reasonable time, the maximum residual was increased to 10^{-4} from 10^{-5}, which was the value used at the other grid sizes.

Two different flow patterns were obtained, depending on the grid size. At the $15 \times 15 \times 7$ the flow pattern at the central plane given in Fig. 5a was obtained; at both the $30 \times 30 \times 14$ and $60 \times 60 \times 28$ grid sizes, the central-plane flow pattern given in Fig. 5b was obtained. For the pattern shown in Fig. 5a, the average cold plate Nusselt number was determined to be 3.882, and for that shown in Fig. 5b, it was determined to be 3.545 (this for the $60 \times 60 \times 28$ grid). These computed cold-face Nusselt numbers are very close to the two measured cold-face Nusselt numbers (which were 3.92 and 3.51, respectively), and so we tentatively concluded that the two different Nusselt numbers observed resulted from there being two solutions, with these two different flow patterns, each with a different Nusselt number.

Examination of the two patterns in Fig. 5 shows that one can be obtained from the other, simply by rotating the flow field through 180° about the centre of the cell. Thus the two flow fields are not really independent. This was confirmed when it was discovered that the cold-face Nusselt number of one solution was essentially equal to the hot-face Nusselt number of the other. This being the case, one can get an improved computed cold-face Nusselt number from the hot-face Nusselt number obtained with the more refined $60 \times 60 \times 28$ grid: this gave $Nu = 3.933$, which compares favourably with the $Nu = 3.9$ mode experimental value of $Nu = 3.949 \pm 0.035$. At the same time the cold-face Nusselt number obtained with the $60 \times 60 \times 28$ grid was 3.545, which compares favourably with the $Nu = 3.5$ mode experimental value of $Nu = 3.510 \pm 0.053$. Interestingly, the average of the cold-face and hot-face Nusselt numbers is the same for both flow patterns; based on the $60 \times 60 \times 28$ grid, it is $Nu = 3.739$. Since in the adiabatic side-wall boundary condition case the two Nusselt numbers have to be equal, the experimental observation of two Nusselt numbers at $Ra = 10^5$ may be an artifact of the LTP boundary condition used in the present experiments.

Neither of the two flow fields follows the lines of any flow-field that has been previously reported. It is clear from Fig. 5 that the flow is fully three-dimensional, in the sense that very substantial amounts of flow has to come into play from the third dimension in order to satisfy continuity. Since the two fields are so closely-related, it is really only necessary to describe one of them. Examining the flow-field shown in Fig. 5a, one finds that, after falling down along the two walls not seen in the drawing (because they are in front of and behind the plane of the drawing), the flow merges at an off-centre

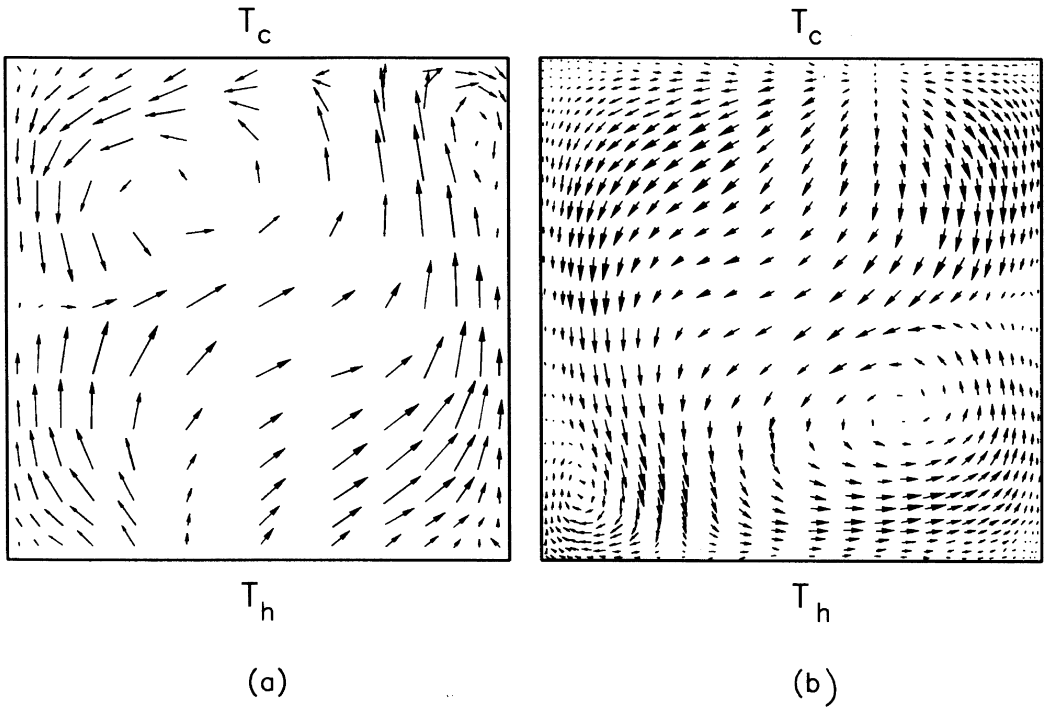

Fig. 5. Velocity plot at the symmetry plane of the flow-fields computed at $\varphi = 0°$ and $Ra = 10^5$. The upper part (a) was computed using a $15 \times 15 \times 7$ grid size, and the lower part (b) using a $30 \times 30 \times 14$ grid size.

location on the hot face and then splits into two components. One rises up the right hand side-wall before going off into the third dimension for its descent down the unseen side-walls, in the process forming a small eddy in the upper right hand corner. The other flow component also rises, but only halfway up the cavity, at which point it makes a sharp right turn and continues into a second, larger eddy that encompasses the upper left hand corner of the cell, at the same time delivering fluid out into the third direction, for its descent down the unseen side-walls.

We obtained the two different flow patterns (or modes) on changing the grid size, but in the real situation the initial conditions will almost certainly decide which mode will be observed. This is what was found by Gomiciaga et al. [19], who made a detailed study of the effect of initial conditions—in particular, the starting temperature distribution—on the flow pattern. In our simulations, we assumed the initial air temperature was uniformly T_m, the average of the two plate temperatures, and because of the symmetry of this condition, some extraneous factor, like a round-off error at an early point in the convergence process, will decide which flow pattern will emerge. In practice, however, the starting temperature profile will be biassed toward one plate or the other, and this will almost certainly be the deciding factor.

This latter observation could explain why we found that the mean temperature T_m was so important in deciding which mode would be observed. In the experiments, the particular Ra of 10^5, was approached by raising the pressure in the pressure vessel. This would bring in a slug of air at a temperature slightly above room temperature, or about 300 K, from the University's compressed air line, changing the tank temperature to that temperature for a short period. During this period, the air would bleed into the cubical cavity. This slug of air could be less than or greater than T_m, depending on the T_m setting, so that, in a relative sense, the initial temperature distribution would be strongly effected by the value of T_m. For one of the two nominal setting of T_m, namely $T_m = 298$ K, the cubical cavity initially contained air above the mean temperature, and for the other setting, of $T_m = 308$ K, the cavity initially contained air decidedly below the mean temperature. These predictions are in keeping with the experimental finding that all of the $T_m = 308$ K settings produced the $Nu = 3.9$ mode and all but one of the $T_m = 298$ K settings produced the $Nu = 3.5$ mode.

Turning now to the Nu vs Ra relation at $\varphi = 0^\circ$ in Fig. 4a, the data points at $Ra = 10^8$, 10^7, 10^6, and the 3.9 mode point at $Ra = 10^5$, were found to be fitted to within 1.6% by

$$Nu = 0.1194 Ra^{0.3021} \tag{3}$$

while the data points at $Ra = 10^4$, 4×10^4 and the 3.5 mode point at $Ra = 10^5$ are fitted to within 0.6% by the equation

$$Nu = 1 + 2.5135 \times 10^{-5} Ra \tag{4}$$

There is a clear change in slope around $Ra = 10^5$, which, interestingly, is where there are two stable solutions. There may be a transition around there from one pattern to another.

Also shown in Fig. 4a is a plot of the multi-purpose, engineering equation recommended by Raithby and Hollands [21] for the 'heated-from-below' enclosure of arbitrary cross-section and Prandtl number. In this equation, Nu depend on the cavity cross-section only through the critical Rayleigh number Ra_c for the cavity, which, for the present case of the square cross-section with LTP side-walls is $Ra_c = 6974$. The agreement is about as good as one might expect from using such a multi-purpose equation. One feature may however be noted: the multi-purpose equation has the larger Ra asymptote $Nu = 0.0555 Ra^{1/3}$. Since the data and the equation appear to be roughly asymptotic to each other at high Ra, we conclude that the data are not inconsistent with there being a one third slope asymptote at high Ra. Moreover it may be speculated that Nu may approach that for layer of fluid heated from below and of infinite horizontal extent; in other words, at very high Ra, the presence of the side-walls is inconsequential.

3.3. Results for $\varphi = 45^\circ$

Plotted in Fig. 4b, the data for the 45° angular setting do not tend to fall along a single line on a log-log plot, at least not for the whole range in Ra. On the other hand the three data point at $Ra = 10^6$, 10^7 and 10^8 fall very close (within 0.2%) to the straight line

$$Nu = 0.1492 Ra^{0.2955} \tag{5}$$

while the three data points at $Ra = 10^4$, 4×10^4 and 10^5 are closely fitted (within 0.2%) by

$$Nu = 0.07309 Ra^{0.3358} \tag{6}$$

One very interesting observation that can be made about these results is that with the exceptions of $Ra = 10^5$ and $\varphi = 0^\circ$, at any given Ra except 10^5, the Nusselt number at $\varphi = 45^\circ$ is greater than that at either $\varphi = 0^\circ$ or $\varphi = 90^\circ$. This is contrary to the various angular scaling laws that have been recommended [20]. It is also different from what Kuyper et al. [15] (and other workers cited by them) found for 2D flow in a square cavity with adiabatic side-walls; they found that for $Ra \leqslant 2.77 \times 10^5$, Nu at $\varphi = 45^\circ$ is indeed greater than that at $\varphi = 90^\circ$, but for $Ra \geqslant 2.77 \times 10^5$, they found Nu at $\varphi = 45^\circ$ to be less than that at $\varphi = 90^\circ$. For example, at $Ra = 10^7$, Kuyper et al. [15] found the Nu at $\varphi = 45^\circ$ to be about 8% less than the corresponding value at $\varphi = 90^\circ$, while the present data show the Nu at $\varphi = 45^\circ$ to be 34.7% greater than the corresponding value at $\varphi = 90^\circ$. Similar differences are found with the square-cavity experimental data of

Hamady et al. [9]. The differences in the angular effects are larger by a factor of about 30 than the experimental errors, and must therefore be attributable to the different shapes of cell (square vs cubic) and the different thermal boundary conditions.

4. Procedures for CFD simulations

Workers wishing to compare these results to the predictions of their CFD code are advised to follow certain recommendations relating to fluid property values, which are based upon the findings of Leong et al. [12]. These workers carried out simulations for $Ra = 40\,000$ at all three angular settings, using a commercial 3D CFD code. They found that treating the fluid properties as invariant with temperature (and making the Boussinesq approximation) gave results close to the measured results: nonetheless, at two of the three angular settings, the difference between the simulated and measured Nusselt numbers was greater than the 95% confidence limits, and yet such a difference would be expected only one out of twenty times. The CFD simulations were repeated, this time with the code taking into account the variation of k, μ, β, and ρ with temperature. This gave much closer agreement, the average difference in the Nu being 0.4% and the maximum difference (occurring at $\varphi = 0^\circ$) being 0.55%. None of the three tests had the difference greater than the 95% confidence limits.

That a variable-property code is needed to obtain results within the experimental range 19 out of 20 times means that the actual temperatures, pressures and dimensions used in the code have to match those in the experiment. The temperature conditions in the 18 measurements that were used in the present experiments varied somewhat, but if one were to do the simulations at the average of the 18 temperature settings, this should give an accurate value to compare to the measured Nusselt number. (The alternative is to do 18 simulations and average the resultant Nusselt numbers, but this would needlessly require many simulations.) Also, the cavity dimension and the pressure should match those of the experiments. Thus we recommend that CFD simulations be carried out in a primitive variable formulation with $T_c = 300$ K, $T_h = 307$ K and $L = 0.1272$ m, and the pressure P equal to that which will give the desired Rayleigh number. In this latter process, the k, μ, β and c_p in the defining equation for Ra should be evaluated at T_m and P, and the ideal gas law should be used to evaluate ρ at the T_m and the pressure in question. Essentially any of the literature equations that model the air property-variation may be used. That is, provided that for the Rayleigh number evaluation, one uses these same literature equations to evaluate the properties at T_m and P, the result should be independent of which equations were actually chosen.

5. Conclusions

At each of the three values of the inclination angle φ, Table 1 gives experimental values of the average cold-plate Nusselt number at Rayleigh numbers running up to 10^8, for the benchmark problem defined by Leong et al. [12] namely the differentially-heated, air-filled cubical cavity having a linear temperature distribution from the cold to the hot isothermal plates, as shown in Fig. 1. The Table includes the relevant 95% confidence-limit uncertainties in the quantities, which are typically about 1% of the Nusselt number. These confidence limits have been established using well-established methods for assessing experimental error, and they have been validated by comparing the measured Nusselt number with essentially exact CFD solutions obtainable at low Ra ($Ra = 40\,000$). It is recommended that workers interested in testing their codes against these data should do their simulations using primitive variables and at the experimental conditions, in a non-Boussinesq simulation that lets the air properties vary from point to point, according to the local temperature. By following these steps, one should get a value that lies within the noted confidence limits, 19 times out of 20.

At $Ra = 10^5$ and $\varphi = 0^\circ$, there are two steady state solutions to the governing equations, each having a different cold-face Nusselt number, and this is why two Nusselt number values are given at this Rayleigh number in Table 1. Which solution (or mode) arises in practice appears to depend on the assumed initial temperature profile. The rather complex, fully-3D flow fields in the two modes are more-or-less images of each other, so that when one of the two Nusselt numbers applies at the cold-face, the other applies at the hot face, and vice-versa. This bistable condition was not observed at any of the other Rayleigh number-angular settings; if they do exist at the other settings tested, the difference in their corresponding Nusselt numbers must be less than the above-stated accuracy of the experiments.

For the same Rayleigh number, the observed Nusselt number at $\varphi = 45^\circ$ was found to generally exceed the corresponding Nusselt number values at both $\varphi = 0^\circ$ and $\varphi = 90^\circ$ for all cases except the heated from below case at $Ra = 10^5$. This rather unexpected result is (over most of the relevant Rayleigh number range) different from what has previously been found for the 2D square cavity with adiabatic side-walls.

It is recognized that experimental results at Rayleigh numbers greater than 10^8 are required for testing turbulence models. Now that the physical-nature of a suitable benchmark problem has been demonstrated,

measurements at higher *Ra* would seem to be a worthy subject for further experimental work.

Acknowledgements

This work was supported by a Natural Sciences and Engineering Research Council (NSERC) Canada Scholarship to W. H. Leong, and also by a Research Grant from NSERC. We also wish to thank Marius Van Reenan for his assistance in designing and trouble-shooting the apparatus.

References

[1] G. de Vahl Davis, Natural convection of air in a square cavity: a bench mark numerical solution, Int. J. Numer. Methods Fluids 3 (1983) 249–264.

[2] P. Le Quere, Accurate solutions to the square thermally driven cavity at high Rayleigh number, Computers Fluids 20 (1) (1991) 29–41.

[3] S.M. ElSherbiny, K.G.T. Hollands, G.D. Raithby, Effect of thermal boundary conditions on natural convection in vertical and inclined air layers, J. Heat Transfer 104 (1982) 515–520.

[4] F. Penot, A. N'Dame, P. LeQuere, Investigation of the route to turbulence in a vertical differentially heated cavity, in: Proceedings of the Ninth International Heat Transfer Conference, vol. 2, Jerusalem, 1990, 417–422.

[5] R. Viskanta, D.M. Kim, C. Gau, Three-dimensional natural convection heat transfer of a liquid metal in a cavity, Int. J. Heat Mass Transfer 29 (3) (1986) 475–485.

[6] I.J. Opstelten, R.A.W.M. Henkes, C.J. Hoogendoorn, On instability mechanisms of the natural convection flow in a side-heated cubical enclosure, First European Conference on Thermal Sciences, vol. 3, 1992, pp. 523–529.

[7] F. Yguel, J.J. Vullierme, Experimental study of high Rayleigh number three-dimensional natural convection in air, in: Significant Questions in Buoyancy Affected Enclosure or Cavity Flows, HTD-60, The American Society of Mechanical Engineers, New York, 1986, pp. 37–44.

[8] A.M. Lankhorst, C.J. Hoogendoorn, Three-dimensional numerical calculations of high Rayleigh number natural convective flows in enclosed cavities, in: Proceedings of the 1988 National Heat Transfer Conference, Heat Transfer Division, American Society of Mechanical Engineers, New York, 1988, pp. 463–470.

[9] F.J Hamady, J.R. Lloyd, H.Q. Yang, K.T. Yang, Study of local natural convection heat transfer in an inclined enclosure, Int. J. Heat Mass Transfer 32 (9) (1989) 1697–1708.

[10] T. Fusegi, J.M. Hyun, K. Kuwahara, B. Farouk, A numerical study of three-dimensional natural convection in a differentially heated cubical enclosure, Int. J. Heat Mass Transfer 34 (6) (1991) 1543–1557.

[11] Y. Le Peutrec, G. Lauriat, Effects of the heat transfer at the side walls on natural convection in cavities, J. Heat Transfer 112 (1990) 370–378.

[12] W.H. Leong, K.G.T. Hollands, A.P. Brunger, On a physically-realizable benchmark problem in internal natural convection, Int. J. Heat Mass Transfer 41 (23) (1997) 3817–3828.

[13] G.D. Raithby, H.H. Wong, Heat transfer by natural convection across vertical air layers, Num. Heat Transfer 4 (1981) 447–457.

[14] J.L. Lage, A. Bejan, The Ra–Pr domain of laminar natural convection in an enclosure heated from the side, Numer. Heat Transfer Part A 19 (1991) 21–24.

[15] R.A. Kuyper, Th.H. Van Der Meer, C.J. Hoogendoorn, R.A.W.M. Henkes, Numerical study of laminar and turbulent natural convection in an inclined square cavity, Int. J. Heat Mass Transfer 36 (11) (1993) 2899–2911.

[16] H. Ozoe, K. Yamamoto, S.W. Churchill, H. Sayama, Three-dimensional, numerical analysis of laminar natural convection in a confined fluid heated from below, J. Heat Transfer 98 (2) (1976) 202–207.

[17] A.M.C. Chan, S. Banerjee, A numerical study of three-dimensional roll cells within rigid boundaries, J. Heat Transfer 101 (2) (1979) 233–243.

[18] H.Q. Yang, K.T. Yang, J.R. Lloyd, Three-dimensional bimodal buoyant flow transitions in tilted enclosures, Int. J. Heat and Fluid Flow 9 (2) (1988) 90–97.

[19] R. Gomiciaga, E. Ramos, J. Rojas, M. Yianneskis, Natural convection flow regimes in a cavity, in: Proceedings of the Third U.K. National Incorporating First European Conference on Thermal Sciences, vol. 1, 1992, pp. 491–497.

[20] G.D. Raithby, K.G.T. Hollands, Natural convection, in: W.M. Rohsenow, J.P. Hartnett, E.N. Ganic (Eds.), Handbook of Heat Transfer Fundamentals, 2nd edn., McGraw-Hill, New York, 1985, chap. 6, pp. 6-51–6-52.

[21] K.G.T. Hollands, Multi-Prandtl number correlation equations for natural convection in layers and enclosures, Int. J. Heat Mass Transfer 27 (3) (1984) 466–468.